Crystal structure of *S*-glutathiolated carbonic anhydrase III

Robert J. Mallis[a], Bradley W. Poland[a,1], Tapan K. Chatterjee[b], Rory A. Fisher[b], Steven Darmawan[a], Richard B. Honzatko[a], James A. Thomas[a,*]

[a] *Department of Biochemistry, Biophysics and Molecular Biology, 1210 Molecular Biology Bldg., Iowa State University, Ames, IA 50011, USA*
[b] *Department of Pharmacology, University of Iowa, Iowa City, IA 52242, USA*

Received 13 April 2000; revised 18 August 2000; accepted 18 August 2000

Edited by Hans Eklund

Abstract ***S*-Glutathiolation of carbonic anhydrase III (CAIII) occurs rapidly in hepatocytes under oxidative stress. The crystal structure of the *S*-glutathiolated CAIII from rat liver reveals covalent adducts on cysteines 183 and 188. Electrostatic charge and steric contacts at each modification site inversely correlate with the relative rates of reactivity of these cysteines toward glutathione (GSH). Diffuse electron density associated with the GSH adducts suggests a lack of preferred bonding interactions between CAIII and the glutathionyl moieties. Hence, the GSH adducts are available for binding by a protein capable of reducing this mixed disulfide. These properties are consistent with the participation of CAIII in the protection/recovery from the damaging effects of oxidative agents.** © **2000 Federation of European Biochemical Societies. Published by Elsevier Science B.V. All rights reserved.**

Key words: Oxidative stress; Protein oxidation; Carbonic anhydrase; Sulfhydryl reactivity; Rat liver; *S*-Glutathiolation

1. Introduction

Oxidative modifications of protein sulfhydryls by *S*-glutathiolation, *S*-nitrosylation, protein disulfide formation and irreversible oxidation have become increasingly important as components of redox-mediated cellular processes that include both regulatory and damage outcomes [1–3]. In particular, *S*-glutathiolation, the formation of mixed disulfides between proteins and glutathione (GSH), occurs rapidly in response to many types of oxidative stress in a wide variety of cell types [4–6]. Indeed, *S*-glutathiolation may be one of the earliest cellular responses to oxidative insult and it may be an essential component of cellular antioxidant defense during such insults. As disulfide bond formation is reversible in vivo, *S*-glutathiolation is a transient event. Protein structure probably plays a role in the reactivity of protein sulfhydryls in *S*-glutathiolation and subsequent reduction of *S*-thiolated proteins by either low molecular weight thiols or by dithiol proteins such as glutaredoxin (GRX, also known as thioltransferase) and thioredoxin (TRX) [5–8]. While structures of proteins that use GSH as a cofactor are well known, e.g. glutathione *S*-transferase [9], glutathione reductase [10] and GRX [8], no structure is available to date of a functional, *S*-glutathiolated intracellular protein in which GSH does not function as a cofactor. It is not known whether sites of *S*-glutathiolation have a special binding affinity for GSH or if the GSH adduct, once formed, adopts a specific conformation that facilitates its reduction.

In male hepatocytes approximately 5% of the soluble protein is carbonic anhydrase III (CAIII) [11], and it is among the first proteins to become *S*-glutathiolated in response to oxidative stress [12]. Two surface cysteines (residues 183 and 188) are amenable to *S*-glutathiolation in vitro and in vivo [11,12]. Recent evidence suggests that the expression of CAIII in NIH-3T3 cells (these cells normally do not express CAIII) may defend against hydrogen-peroxide induced apoptosis [13]. Expression of the protein is also increased in experimental alcoholic liver disease [14].

This report contains the crystal structure of *S*-glutathiolated CAIII, in which both Cys183 and Cys188 are *S*-glutathiolated. The absence of specific interactions between the surface of CAIII and the GSH adducts in the crystal structure suggests a general mechanism of *S*-thiolation, in which GSH reacts spontaneously with thiol groups exposed to the aqueous cellular environment. In addition, we propose a general mechanism of dethiolation, in which the recognition of the GSH adduct alone is the overriding determinant in the catalytic reduction of protein mixed disulfides.

2. Materials and methods

2.1. Sequencing of cDNA for rat liver CAIII

Polymerase chain reaction (PCR) amplification of Marathon-Ready cDNAs (Clontech Laboratories) employed the manufacturer's standard protocols. Forward (GCGTGGTGAAGGAGCCAT) and reverse (CCTCTCTCTGGACCCTACCGA) primers for PCR were designed using the cDNA sequence for rat muscle CAIII [15]. The above primers and their DNA complements were used in sequencing the expressed portion of the gene. Each position in the sequence was determined by at least two sequencing reactions.

2.2. Purification of rat liver CAIII

Pure *S*-glutathiolated CAIII was obtained directly from rat liver, using the protocol of Chai et al. [12], subject to the following modifications. Instead of using a second pass through the DEAE column, protein from the DEAE Sepharose column was separated in a Rotofor preparative isoelectric focusing chamber using ampholytes of pH 4.0–8.0. The most homogeneous fractions from several enzyme preparations, as determined by thin gel isoelectric focusing (IEF), were pooled and run a second time without additional ampholytes, effectively narrowing the pH range of the separation to pH 6.0–7.5. The most homogeneous fractions were pooled and run a third time without addition of ampholytes, again increasing the resolution of separation. The most homogeneous fractions were pooled and used for crystallographic analysis.

*Corresponding author. Fax: (1)-515-294 0453.
E-mail: jat@iastate.edu

[1] Present address: Howard Hughes Medical Institute, Baylor College of Medicine, Houston, TX 77030, USA.

Abbreviations: GSH, glutathione; GRX, glutaredoxin; TRX, thioredoxin; CAIII, carbonic anhydrase III

PII: S0014-5793(00)02022-6

2.3. Crystallization of S-glutathiolated CAIII

Crystals of *S*-glutathiolated CAIII were grown by the method of hanging drops. Six microliters of a solution containing 10 mg/ml protein, 10% propanol (v/v), 15–20% (w/v) polyethylene glycol 3350 and 100 mM HEPES, pH 7.5, was suspended in a chamber containing a reservoir (0.5 ml) of 10% (v/v) propanol, 15–20% (w/v) polyethylene glycol 3350, and 100 mM HEPES, pH 7.5. Crystals (space group $P2_1$) of equal dimensions (0.4–0.5 mm) grew within a week at room temperature.

2.4. X-ray diffraction data collection, structure determination and refinement

Data were collected from a single crystal on a Siemens area detector/rotating anode at Iowa State University, using a graphite monochromater and copper, K_α radiation. The data were reduced by XENGEN [16]. The structure of *S*-glutathiolated CAIII was determined by molecular replacement, using the structure of CAII (Protein Data Bank accession identifier, 3CA2). Programs from the CCP4 suite [17] were used in generating rotation and translation functions, each of which provided unambiguous peaks for the correct orientation and position of CAIII in the $P2_1$ reference frame. Rigid body refinement of the CAII model against data to 2.8 Å resulted in an *R*-factor of 0.30. A single cycle of simulated annealing, using XPLOR [18] in combination with geometry and energy parameters of Engh and Huber [19], reduced the *R*-factor to 0.25.

A model was fit to the resulting electron density map, using TOM [20], a Silicon Graphics workstation, and the amino acid sequence shown in Fig. 1. Ensuing rounds of refinement, included the restrained refinement of individual thermal parameters, the active site Zn^{2+} and water molecules. Water molecules were not introduced in the vicinity of Cys183 and Cys188, sites of *S*-glutathiolation, due to the disorder of the GSH adducts. The final rounds of model building and refinement were devoted to the modeling of GSH adducts to the above cysteines. As described below, although the disulfide linkages of adducts were clearly revealed in omit difference maps, electron density beyond the disulfide linkage was diffuse, implying multiple conformations for each adduct. Coordinates are available from the Protein Data Bank, accession number 1FLJ.

3. Results

3.1. Amino acid sequence of rat liver CAIII

The amino acid sequence, as derived from the cDNA of rat liver CAIII, is shown in Fig. 1 along with published sequences for rat muscle [15] and bovine muscle CAIII [21]. Our crystal structure of the rat liver protein confirms the sequence of the five variant positions of the liver enzyme as shown in Fig. 1. The numbering of amino acids in the sequence for the rat liver enzyme corresponds to the standard set for carbonic anhydrase isozymes [22].

3.2. Purity and stability of S-glutathiolated CAIII

Purification of completely *S*-glutathiolated CAIII from 300 g of rat liver produced 1.2 mg of purified *S*-glutathiolated CAIII. The *S*-glutathiolated CAIII used in crystallization experiments has the same electrophoretic mobility as the material characterized by Chai et al. [11], in which both Cys183 and Cys188 were *S*-glutathiolated. Fig. 2 shows the purity of the protein at successive steps in purification. The isoelectric point of the purified *S*-glutathiolated protein provides evidence that at least 99% of the protein was completely *S*-glutathiolated on both reactive cysteines. There is very little contamination by the reduced form of the protein as indicated by the arrow in Fig. 2. The protein also gave a single band on sodium dodecyl sulfate–polyacrylamide gel electrophoresis. *S*-Glutathiolation had no effect on carbonic anhydrase activity. *S*-Glutathiolated CAIII was stable under conditions of crystallization, as material recovered from crystals had the same p*I* as the starting material.

3.3. Crystal structure of S-glutathiolated CAII

Crystals of *S*-glutathiolated CAIII belong to the space group $P2_1$ ($a = 41.25$, $b = 44.73$, $c = 66.91$ and $\beta = 99.73°$) and diffract to a nominal resolution of 1.8 Å ($\langle I/\sigma I \rangle = 2$). Statistics of data collection and refinement are in Table 1. The method of Luzzati indicates that the uncertainty in coordinates of atoms is approximately 0.15 Å [23]. Thermal parameters vary from 5 to 47 Å^2. On the basis of PROCHECK [24], all residues fall within the generously allowed region of the Ramachandran plot and the stereochemistry of the refined model is

```
                10        20        30        40        50        60
RL  -AKEWGYASHNGPEHWHELYPIAKGDNQSPIELHTKDIRHDPSLQPWSVSYDPGSAKTIL
RM  -AKEWGYCSHNGPEHWHELYPIAKGDNQSPIELHTKDIRHDPSLQPWSVSYDPGSAKTIL
BM  -AKEWGYADHNGPDHWHELFPNAKGENQSPIELNTKEINHDPSLKPWTASYDPGSAKTIL

                70        80        90        100       110       120
RL  NNGKTCRVVFDDTFDRSMLRGGPLSGPYRLRQFHLHWGSSDDHGSEHTVDGVKYAAELHL
RM  NNGKTCRVVFDDTFDRSMLRGGPLSGPYRLRQFHLHWGSSDDHGSEHTVDGVKYAAELHL
BM  NNGKTCRVVFDDTYDRSMLRGGPLAAPYRLRQFHLHWGSSDDHGSEHSVDGVKYAAELHL

                130       140       150       160       170       180
RL  VHWNP-KYNTFGEALKQPDGIAVVGIFLKIGREKGEFQILLDALDKIKTKGKEAPFNHFD
RM  VHWNP-KYNTSEEALKQPDGIAVVGIFLKIGREKGEFQILLDALDKIKTKGKEAPFNHFD
BM  VHWNS-KYNSYATALKQADGIAVVGVFLKIGREKGEFQLLLDALDKIKTKGKEAPFNNFN

      ⇓   ⇓ 190       200       210       220       230       240
RL  PSCLFPACRDYWTYHGSFTTPPCEECIVWLLLKEPMTVSSDQMAKLRSLFASAENEPPVP
RM  PSCLFPACRDYWTYHGSFTTPPCEECIVWLLLKEPMTVSSDQMANVRSLFASAENEPPVP
BM  PSCLFPACRDYWTYHGSFTTPPCEECIVWLLLKEPITVSSDQIAKLRTLYSSAENEPPVP

                250       260
RL  LVGNWRPPQPIKGRVVRASFK
RM  LVGNWRPPQPIKGRVVRASFK
BM  LVRNWRPPQPIKGRIVKASFK
```

Fig. 1. Amino acid sequence of CAIII. The amino acid sequences of rat liver CAIII (RL) (GenBank accession number AF037072), rat muscle CAIII (RM) [15] and bovine muscle CAIII (BM) [21] are aligned. Differences between the two rat isoforms are enclosed in dark boxes. *S*-Glutathiolated cysteines in the crystal structure are marked (⇓).

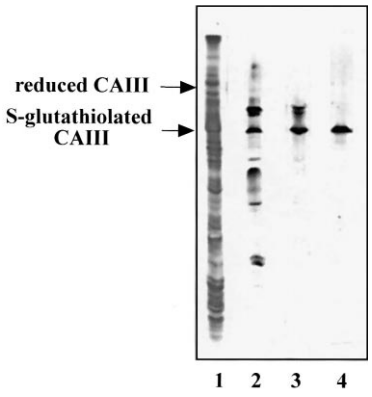

Fig. 2. Purity of *S*-glutathiolated CAIII. IEF gel, pH 4–8, of successive steps of purification of *S*-glutathiolated CAIII. Lane 1, the soluble fraction of the rat liver preparation (see Section 2); lane 2, the soluble fraction after DEAE–trisacryl column chromatography; lane 3, the preparation after first preparative IEF (Rotofor) run; lane 4, the purified protein. Arrows show the isoelectric point for reduced and fully *S*-glutathiolated (two sites) CAIII.

better than that obtained from a typical structure of 2.0 Å resolution.

C^{α} atoms of *S*-glutathiolated CAIII and reduced CAIII [21] superimpose with a root-mean-squared deviation of 0.64 Å (Fig. 3). The active sites of the two structures are essentially identical, in harmony with the absence of an effect of *S*-glutathiolation or alkylation [25] on CAIII activity. GSH adducts do not perturb C^{α} atoms in the vicinity of Cys183 and Cys188. Even side chains near the two modified cysteines showed little movement in response to glutathiolation. Hence the structures of *S*-glutathiolated CAIII and reduced bovine muscle CAIII [21] are very similar.

The electron density in omit maps reveals mixed disulfide linkages at cysteines 183 and 188. However, diffuse electron density beyond the sulfur atom of the GSH moiety is consistent with multiple conformations at positions beyond the sulfur atom of the GSH. The GSH moiety at position 183 (labeled GSH1 in Fig. 3A and detailed in Fig. 3B) has two conformations which differ by approximately 120° in χ^1 of Cys183. The two conformations were present in approximately equal amounts as judged from the relatively equal electron density for the sulfur atoms of each adduct (Fig. 3C). In one conformation (GSH1) the backbone carbonyl of the cysteine residue hydrogen bonds directly with the backbone amide of Asp180 and with backbone carbonyl 178 through a bridging water molecule. In addition, the carbonyl of the γ-glutamyl group of GSH1 hydrogen bonds with His178 through a bridging water molecule. The amino group of the γ-glutamyl group of GSH1 and the side chain of Glu156 probably interact electrostatically, but the interaction does not perturb the existing salt link between the side chains of Glu156 and Lys154. The GSH adduct associated with the second orientation of the disulfide linkage is so poorly ordered (Fig. 3C), a definitive conformation cannot be assigned. The carboxyl terminus of GSH1, however, could interact electrostatically with the side chain of Arg189 (but not by way of a stable salt-link), and the amino terminus of GSH1 may interact with an arginine from a CAIII molecule related by crystal symmetry. The GSH adduct at Cys188 (labeled GSH2 in Fig. 3A and detailed in Fig. 3D) has a density for only a single orientation of the disulfide linkage; the rest of the adduct, however, is disordered. The GSH adduct potentially interacts with Asp at position 188 and might interact with Arg189, although there is no evidence for a stable salt link.

Conformation 1 of Cys183 (GSH1) puts the GSH adduct in a shallow cleft which limits the number of sterically allowed conformations (Fig. 4A). The GSH1 conformer is limited in its rotation about the S^{γ}–S^{γ} bond mainly by Glu156 and the peptide chain of Asp180. It is also limited in rotation about the C^{β}–S^{γ} bond by Ile159 and by Cys183. Conformation 2 of Cys183 (GSH1) puts the GSH adduct in a region of few steric constraints, allowing it more freedom of movement than conformer 1 (Fig. 4B). The area around Cys188 and GSH2 places almost no limitations on the conformation of the GSH adduct. The highest electron density levels are associated with the most conformationally constrained adduct (conformer 1 of GSH1 of Cys183).

With respect to the reactivity of the *S*-glutathiolated sites, Cys188 (GSH2) places no apparent limits on the approach of a nucleophile during dethiolation of the protein. On the other hand, Ile159 could block S^{γ} of GSH1 from an approaching nucleophile (Fig. 4A). Although conformation 2 of Cys183 places no obstacles in the path of an approaching nucleophile (Fig. 4B), steric effects in conformation 1 may account for the slower dethiolation of one of the two adduct sites on CAIII [11].

Significantly, the disorder of the attached GSH moieties correlates well with the chemical reactivity of the two cysteines. One cysteine is more reactive in glutathiolation reactions [2,11], alkylation reactions with a negatively charged alkylating agent [26] and dethiolation reactions [11]. A recent report identified the most reactive cysteine as Cys188 [2].

The surface charge characteristics of CAIII may also influence the reactivity of the protein sulfhydryl. Fig. 5 shows a model of the surface at the two reactive sulfhydryls and the calculated surface charge distribution around each site. In Fig. 5 the light gray areas have a negative charge, the dark gray areas have a positive charge and the white areas are neutral. In order to indicate the direction of the mixed disulfide bonds at the two cysteines, small white dots indicate the position of the sulfur atom from the GSH adduct. Both reactive cysteines

Table 1
Statistics of data collection and refinement

Resolution limit (Å) of data	1.8
No. of measurements	44 741
No. of unique reflections	20 193
Completeness of data (%)	90
Completeness of data in last shell	79
R_{sym} [a]	5.4
Resolution range of refinement (Å)	5–1.8
No. of reflections in refinement[b]	14 426
Total number of atoms	3142
Total number of solvent sites	200
R-factor[c]	0.155
R_{free} [d]	0.213
Mean *B* values (Å^2)	
Entire protein	13
Glutathione adducts	65
Root mean squared deviations	
Bond lengths (Å)	0.009
Bond angles (°)	1.51

[a] $R_{sym} = \Sigma_i \Sigma_j |I_{ij} - \langle Ij \rangle| / \Sigma_i \Sigma_j I_{ij}$.
[b] Only reflections with $F_{obs} > 0$ were used in the refinement.
[c] *R*-factor $= \Sigma |F_{obs} - F_{calc}| / \Sigma F_{obs}$, for all reflection $F_{obs} > 0$.
[d] *R*-factor based on 10% of the data excluded from refinement.

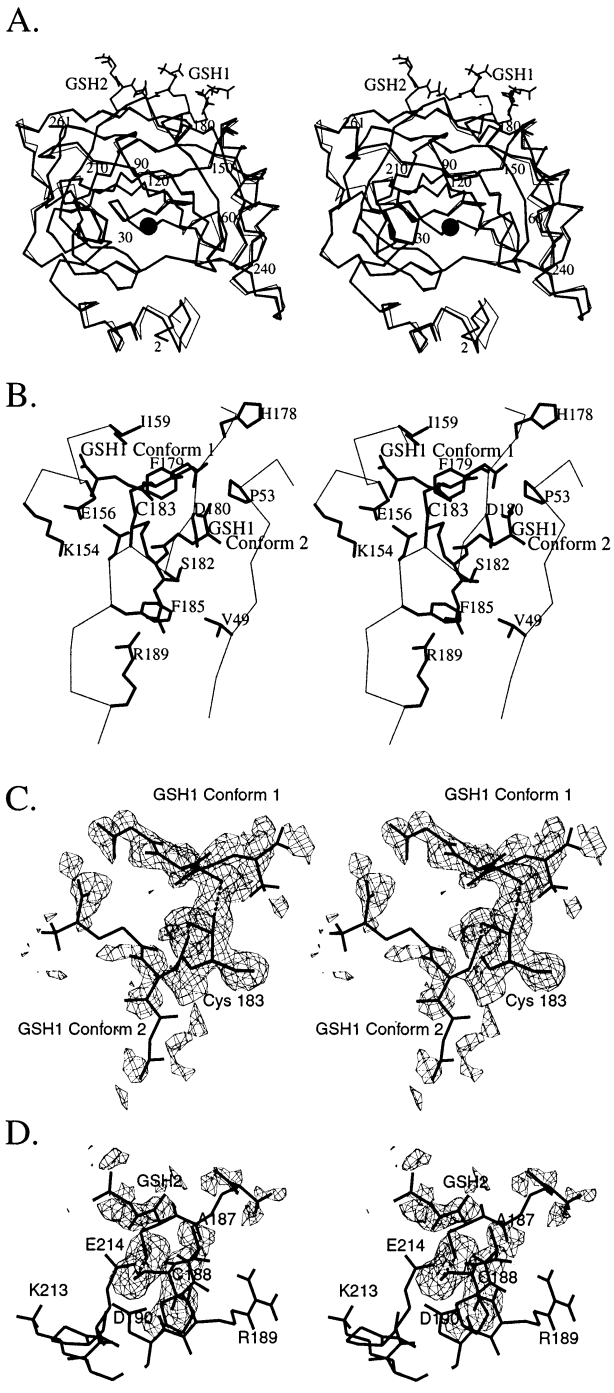

Fig. 3. Structure of *S*-glutathiolated CAIII. A: The superposition of C^{α}-traces of *S*-glutathiolated CAIII (bold line) and reduced bovine CAIII. The filled circle = zinc. Glutathionyl disulfide-bonded adducts at cysteines 183 and 188 are labeled GSH1 and GSH2. B: Close-up view of two conformations of the Cys183 adduct. C: Close-up view as in (B) with electron densities superimposed on the model. The electron density from a $2F_{obs}-F_{calc}$ map around Cys183 and GSH1 in both conformations is shown with a cover radius of 1.5 Å and contoured at 1.2σ. The disulfide linkages for both conformations are visible at contours up to 5σ. The remainder of the GSH adduct in conformation 1 is visible at contour levels less than 3.8σ, while GSH conformation 2 is only visible at less than 2.4σ. D: Close-up view of the Cys188 adduct. The electron density from a $2F_{obs}-F_{calc}$ map around Cys188 and GSH2 is shown at a 1.5 Å cover radius and contoured at 1.2σ. The disulfide linkage is visible at contour levels of 5σ, while the rest of the GSH adduct is only visible at 2.0σ or less. Images for (A) and (B) were generated with RasMol [27], and (C) and (D) were generated with TOM [20].
←

are surrounded primarily by a negatively charged protein surface.

When Cys183 (Fig. 5, bottom) is in conformation 1, the disulfide bond defines a sterically hindered line of approach for an incoming nucleophile. The sulfhydryl resides in a depression in the surface in which the surrounding negative charge is considerably greater (light gray in Fig. 5) than when Cys183 is in conformation 2 (Fig. 5, top). The published structure of reduced CAIII shows Cys183 in conformation 1 [21]. Because this hindered conformation would require interactions between the attacking nucleophile and the protein, it is likely that negatively charged compounds would react more poorly with this site relative to Cys188. The exposed conformation of Cys188 and the lower level of negative charge at this site (Fig. 5) probably account for this residue's similar reactivity with both charged (iodoacetate) and uncharged (iodoacetamide) reagents in alkylation reactions.

4. Discussion

The covalent modifications of CAIII presented here are consistent with rapid, reversible *S*-glutathiolation and dethiolation of surface sulfhydryls during oxidative stress in intact cells. The primary oxidative reaction in CAIII may be a spontaneous (thermodynamically favored) partial oxidation of cysteines to sulfenic acids or thiyl radicals, which then react with cellular GSH to form disulfide adducts [1]. The high concentration of GSH in vivo makes a high-affinity binding site for GSH on the protein unnecessary, and indeed the crystal struc-

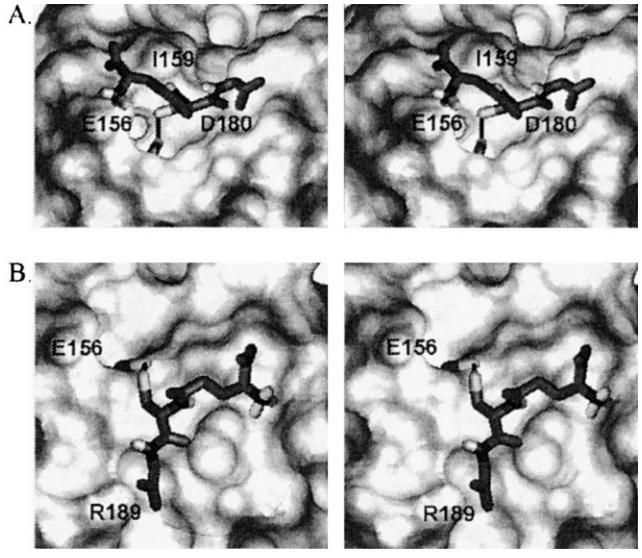

Fig. 4. Stereo, surface representation of *S*-glutathiolated CAIII in the vicinity of the Cys183 adduct. The two conformers of the Cys183 adduct are represented by wireframe models. The disulfide bonds between GSH1 and Cys183 are shown as thin black lines. The view is approximately the same as that in Fig. 3B. The image was generated using MolMol [28]. A: Conformation 1 of the Cys183–GSH1 adduct. This is the same conformation of Cys183 as is found in the reduced bovine CAIII structure [27]. B: Conformation 2 of Cys183–GSH1 adduct.

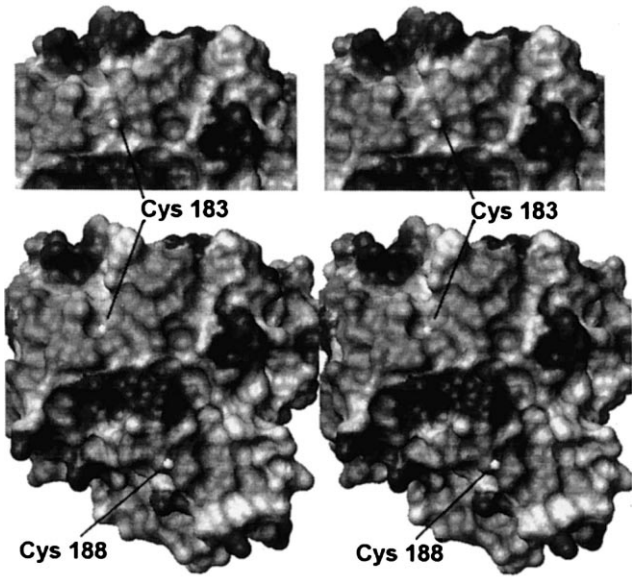

Fig. 5. Electrostatic and solvent-accessible surface representation of CAIII in stereo. Dark gray coloration represents a positive charge, light gray a negative charge and white a neutral charge. The position of S^{γ} of the GSH adducts are indicated by white balls. The lower portion of the figure shows the electrostatic surface of CAIII when the cysteines are in conformation 1. This is the same conformation as that of the reduced bovine CAIII model [21]. The upper portion of the figure shows the surface when Cys183 is in conformation 2. The electrostatic and surface calculations were carried out using MolMol [28], which utilizes the algorithm of Nicholls and Honig [29].

ture provides no evidence for the specific recognition of GSH. In fact, the disordered adduct suggests a lack of direct involvement by CAIII constituents with the processes of thiolation and dethiolation. Surface accessibility, the electrostatic environment, and the absence of specific GSH–protein interactions each contributes to the reactivity of these sulfhydryls. For instance, the most reactive cysteine, Cys188, has a GSH adduct with the least structural order. Evidently, this protein forms a mixed disulfide with GSH in vivo as a result of GSH abundance, rather than the presence of a high-affinity binding site for GSH. Potentially, this mechanistic concept may apply to most reactive protein cysteines.

Dethiolation of *S*-glutathiolated CAIII is catalyzed by proteins containing a dithiol reduction site, i.e. GRX (thioltransferase) or TRX. It was recognized early that each of these proteins has a different specificity for disulfide substrates [7] and recent kinetic data both from our laboratory [5] and from others [6], suggests that GRX is considerably more efficient as a protein dethiolase than is TRX. Modeling studies (not shown here) explain this observation since GRX can easily recognize the GSH adduct on *S*-glutathiolated CAIII without interacting with the surface of the CAIII protein in a significant manner. On the other hand TRX inevitably produced some overlap with the CAIII surface when modeled into the *S*-glutathiolated CAIII structure. This interaction may potentially lead to distortion of the CAIII structure during the action of TRX. Thus, the specificity of the dethiolation process may result from strong interactions between GRX and the GSH adduct, and from a lack of hindering interactions with the protein (CAIII) being reduced. As GRX may need to recognize the GSH adduct in the context of many different surface structures [5,11], extensive interactions between GRX and the protein surface at any one site would likely result in unfavorable interactions at another site.

Acknowledgements: This work was supported by NIH Grant NS 10546 (R.B.H.), NSF Grant MCB-9316244 (R.B.H.) and an American Heart Association Grant (J.A.T.). This is Journal Paper No. J-18025 of the Iowa Agriculture Home Economics Experiment Station, Ames, IA, Project No. 2968.

References

[1] Thomas, J.A., Poland, B. and Honzatko, R. (1995) Arch. Biochem. Biophys. 319, 1–9.
[2] Cabiscol, E. and Levine, R.L. (1996) Proc. Natl. Acad. Sci. USA 93, 4170–4174.
[3] Lander, H.M. (1997) FASEB J. 11, 118–124.
[4] Cabiscol, E. and Levine, R.L. (1995) J. Biol. Chem. 270, 14742–14747.
[5] Jung, C.H. and Thomas, J.A. (1996) Arch. Biochem. Biophys. 335, 61–72.
[6] Gravina, S.A. and Mieyal, J.J. (1993) Biochemistry 32, 3368–3376.
[7] Mannervik, B., Axelsson, K., Sundewall, A.-C. and Holmgren, A. (1983) Biochem. J. 213, 519–523.
[8] Bushweller, J.H., Billeter, M., Holmgren, A. and Wüthrich, K. (1994) J. Mol. Biol. 235, 1585–1597.
[9] Dirr, H., Reinemer, P. and Huber, R. (1994) Eur. J. Biochem. 220, 645–661.
[10] Karplus, A.P. and Shultz, G.E. (1989) J. Mol. Biol. 210, 163–180.
[11] Chai, Y.C., Jung, C.H., Lii, C.K., Ashraf, S.S., Hendrich, S., Wolf, B., Sies, H. and Thomas, J.A. (1991) Arch. Biochem. Biophys. 284, 270–278.
[12] Chai, Y.C., Hendrich, S. and Thomas, J.A. (1994) Arch. Biochem. Biophys. 310, 264–272.
[13] Raisenen, S.R., Lehenkari, P., Tasanen, M., Rahkila, P., Harkonen, P.L. and Vaananen, H.K. (1999) FASEB J. 13, 513–522.
[14] Parkkila, S., Halsted, C.H., Villanueva, J.A., Vaananen, H.K. and Niemela, O. (1999) Dig. Dis. Sci. 44, 2205–2213.
[15] Kelly, C.D., Carter, N.D., Jeffery, S. and Edwards, Y.H. (1988) Biosci. Rep. 8, 401–406.
[16] Howard, A.J., Nielsen, C. and Xuong, N.H. (1985) Methods Enzymol. 114, 452–472.
[17] Collaborative Computational Project No. 4, (1994) Acta Crystallogr. D 50, 760–763.
[18] Brünger, A.T. (1992) XPLOR:version 3.1. A System for X-ray Crystallography and NMR, Yale University Press, New Haven, CT.
[19] Engh, R.A. and Huber, R. (1991) Acta Crystallogr. A 47, 392–400.
[20] Cambillau, C. and Horjales, E. (1987) J. Mol. Graph. 5, 174–177.
[21] Eriksson, A.E. and Liljas, A. (1993) Proteins 16, 29–42.
[22] Deutsch, H.F. (1987) Int. J. Biochem. 19, 101–113.
[23] Luzzati, V. (1952) Acta Crystallogr. 5, 802–810.
[24] Laskowski, R.A., Mac Arthur, M.W., Moss, D.S. and Thornton, J.M. (1993) J. Appl. Crystallogr. 26, 283–291.
[25] Engberg, P. and Lindskog, S. (1986) Eur. J. Biochem. 156, 407–412.
[26] Ji, Y., Akerboom, T.P.M., Sies, H., and Thomas, J.A. (1999), Methods in Enzymology (Lester Packer, Ed.), Vol. 301, pp. 145–151. Academic Press, Orlando, FL.
[27] Sayle, R. and Milner-White, E.J. (1995) Trends Biochem. Sci. 20, 374–375.
[28] Koradi, R., Billeter, M. and Wüthrich, K. (1996) J. Mol. Graph. 14, 51–55.
[29] Nicholls, A. and Honig, B.J. (1990) Comp. Chem. 12, 435–445.